Microstructure and the boson peak in thermally treated In_xO films

Itai Zbeda [1], Ilana Bar [1], and Z. Ovadyahu [2]
[1] *Department of Physics, Ben-Gurion University of the Negev, Beer-Sheva 8410501, Israel*
[2] *Racah Institute of Physics, The Hebrew University, Jerusalem 9190401, Israel*

(Received 18 March 2021; accepted 6 August 2021; published 26 August 2021)

We report on the correlation between the boson peak and the structural changes associated with thermally treating amorphous indium-oxide films. In this process, the resistance of a given sample may decrease by a considerable margin whereas its amorphous structure is preserved. In the present paper, we focus on the changes that result from the heat treatment by employing electron-microscopy, x-ray, and Raman spectroscopy. These techniques were used on films with different stoichiometry and, thus, different carrier concentrations. The main effect of heat treatment is material densification, which presumably results from elimination of microvoids. The densified system presents better wave-function overlap and more efficient connectivity for the current flow. X-ray and electron-beam diffraction experiments indicate that the heat-treated samples show significantly less spatial heterogeneity with only a moderate change in the radial-distribution function metrics. These results are consistent with the changes that occur in the boson-peak characteristics due to annealing as observed in their Raman spectra.

DOI: 10.1103/PhysRevMaterials.5.085602

I. INTRODUCTION

Disorder plays a major role in the properties of solids. The study of disorder is a challenge in terms of being able to control, characterize, and quantify it. A significant effort in this vein was invested in the field of electronic transport. In particular, the need for modifying and quantifying disorder is an essential ingredient in the field of disorder-induced phenomena. Prime examples in this category are the metal-insulator transition and the superconductor-insulator transition. The system resistivity is sometimes used as an empirical measure of disorder in these studies. Electric conductivity of a solid is arguably its most sensitive property, and it may be affected by different means, not all of them may be attributed to disorder. A change in carrier concentration, for example, naturally affects conductivity whereas only a small (and indirect) change in disorder may be incurred in the process.

Restricting the lateral dimensions of the sample has been widely used to increase scattering. This is, in particular, a viable technique to change disorder in transport studies of thin films. However, to introduce strong disorder in a three-dimensional system, one may have to resort to alloying or use a two-component mixture; a granular system. An effective method that was employed to introduce disorder in a metallic system was exposure to neutron or α-particle radiation. This technique was employed in modifying the transport properties of A-15, MgB_2, and other materials by introducing point defects and grain-boundary spacing [1].

A complementary backward procedure is thermal annealing. This is an effective way to reduce disorder when the system is disordered to start with, a common situation in vacuum deposited or quench-cooled systems. Thermal annealing has been successfully used in various transport experiments as a means of fine-tuning the disorder of amorphous indium-oxide (In_xO) films. It has been shown that thermally treating In_xO films may result in resistance change of up to four to five orders of magnitude at room temperature with only a small change in carrier concentration measured by the Hall effect. It seems, therefore, that the huge change in resistance is due to enhanced mobility, suggestive of a less disordered system. The range of disorder attainable with this method allows studies of both sides of the metal insulator and the superconductor-insulator transitions of this material. It was argued that the main reason for the resistance change is densification [2]. This was supported by demonstrating the similarity of the change in the optical gap during thermally annealing In_xO films, and in studies of pressure-induced densification of glasses.

Another property known to be sensitive to disorder in solids is the boson peak (BP), which has been widely studied in amorphous systems and glasses [3–12]. The BP is a feature that appears at the low-energy vibrational-density of states of amorphous and disordered systems. This feature may be resolved by heat-capacity, neutron-scattering experiments, and by Raman spectroscopy. There are several competing theoretical models that purport to account for the mechanism that underlies the BP. The common ingredient in the great majority of them is spatial disorder [4,5,8,13–16]. This makes the characteristics of the BP a relevant probe for monitoring changes in disorder. This is of particular relevance for amorphous systems where quantifying disorder is a challenge. In addition to the lack of long-range order, most amorphous solids exhibit mass density that is lower than their crystalline counterpart. This is presumably due to their being formed by fast cooling from the liquid or gaseous phase [17]. The latter preparation method, quench cooling the material from the vapor phase

onto a cold substrate, usually results in a porous structure that has many microvoids reducing the material bulk specific gravity. Consequently, an appreciable volume change may be affected in these structures upon application of pressure and by thermal treatment [2].

In this paper we attempt to further elucidate these issues using several versions of amorphous indium oxide as a model system for a metallic glass. This allows us to track changes in the BP due to quantifiable changes of disorder. Raman spectroscopy taken from as-made and annealed In_xO films of different composition, reveal significant changes in the BP magnitude and shape. It is noted that Raman spectroscopy may not faithfully convey the detailed shape of the BP as compared with, for example, heat-capacity measurements [18]. However, it is still a viable tool to identify relative changes in the spectra caused by modification of the system structure. Our Raman spectra results are discussed in conjunction with the microstructure information based on x-ray and electron-diffraction experiments made on these samples. In particular, our study illustrates how various aspects of structural disorder affect electronic properties, such as conductivity as compared with their effect on the BP shape and magnitude. The similarities and differences with the behavior of the BP in other glasses were pressure was used to modify the structure are pointed out.

II. EXPERIMENT

A. Samples preparation and characterization

The In_xO films were e-gun evaporated onto room-temperature substrates using a 99.999% pure In_2O_3 sputtering target. Deposition was carried out at the ambience of $3 \pm 0.5\times10^{-5}$- to $4 \pm 0.5\times10^{-4}$-Torr oxygen pressure maintained by leaking 99.9% pure O_2 through a needle valve into the vacuum chamber (base pressure $\simeq 10^{-6}$ Torr). Different substrates were used for the samples prepared for the different measurement techniques. Undoped silicon wafers were used as substrates for electrical measurements, x-ray diffraction (XRD) and Raman spectroscopy measurements. Carbon-coated copper grids were used for transmission electron microscopy (TEM) imaging and electron diffraction. During deposition and thermal treatment the grids were anchored to glass slides by small indium balls pressed onto the glass. The deposited film on the rest of the slide was used for monitoring the sample resistance. X-ray reflectometry (XRR) measurements were performed on samples deposited on 3.8-mm-thick float-glass slides.

Rates of deposition in the range of 0.3-2.5 Å/s were used to produce films with different compositions; The In_xO samples had carrier-concentration N that increases with the ratio of deposition rate to the oxygen partial pressure. For the rate pressures used here N was in the range of 2×10^{19} to 5×10^{21} cm^{-3} as measured by the Hall effect at room temperature using a Hall-bar control sample prepared simultaneously for each sample deposition. The evaporation source to substrate distance in the deposition chamber was 45 ± 1 cm. This yielded films with thickness uniformity of $\pm 2\%$ across a 2×2-cm^2 area. Lateral sizes of samples used for transport measurements was typically 1×2 mm^2 (width $\times$ length, respectively), and 1×1 cm^2 for the Raman spectroscopy. To afford reasonable resolution for electron-microscopy thickness of the films used for TEM work was typically $d = 200 \pm 10$ Å.

Three batches of In_xO with different carrier-concentrations $N = (4 \pm 1)\times10^{19}$, $(1 \pm 0.5)\times10^{20}$, and $(9 \pm 1)\times10^{20}$ cm^{-3} were used for Raman spectroscopy. For structural analysis we used films characterized by the Ioffe-Regel parameter $k_F\ell = (3\pi^2)^{2/3}\frac{\hbar\sigma_{RT}}{e^2N^{1/3}}$ in the range of 0.08–0.4. Here σ_{RT} is the room-temperature conductivity. This range covers the critical value of $k_F\ell = 0.32 \pm 0.2$ where the metal-insulator transition and superconductor-insulator transition of In_xO take place [19,20].

High-resolution TEM images and electron-diffraction patterns were taken with the Philips Tecnai F20 G2 operating at 200 kV. X-ray diffraction and reflectometry were taken with Bruker diffractometer AXS D8 Advance equipped with a Lynexeye XE-T silicon strip detector. The diffractometer has step resolution of 10^{-4} °.

Raman spectroscopy at Ben-Gurion University of the Negev was performed with a home-built ultra-low-frequency Raman microscope confocal system that was assembled and optimized for measurements down to 10 cm^{-1}. The setup employed a single longitudinal mode green laser operating at 532 nm. The laser power used in the measurements was typically 3 mW for a spot diameter of ≈ 2.6 μm. The scattered signal was collected via high throughput 532 longpass nanoedge filters and a single spectrometer [21]. Complementary Raman spectroscopy studies in the Hebrew University were taken with a Renishaw inVia Reflex Spectrometer using a laser beam with either 514- or 785-nm wavelength and edge filter at ≈ 70 cm^{-1}, therefore, these measurements were limited to energies $\gtrsim 80$ cm^{-1}.

B. The thermal-treatment protocol

The protocol we routinely use for monitoring the annealing process involves the following steps: After removal from the deposition chamber, the sample was mounted onto a heat stage in a small vacuum cell wired to make contacts with the sample for electrical measurements and a thermocouple attached to the sample stage as a thermometer. Resistance measurements were performed by a two-terminal technique using either the computer-controlled HP34410A multimeter or the Keithley K617. Next the heating stage is energized, and the resistance and temperature are continuously measured throughout the heating, relaxation, and cooling periods. A typical annealing cycle is illustrated in Fig. 1: The sharp changes in the sample resistance R when the heating is turned on and off are mostly due to the temperature-dependent coefficient that in this disorder regime is negative. However, during the time that the temperature has settled at the target value for annealing, R continues to slowly decrease. Then, after cool down to room temperature, the resistance slowly increases approaching an asymptotic value that, ordinarily, is smaller than at the start of the heat-treatment cycle.

These slow $\Delta R(t)$ reflect changes in the system volume (densification and rarefaction, respectively). The change in volume in the process of thermally treating In_xO films was demonstrated in an interference experiment using a

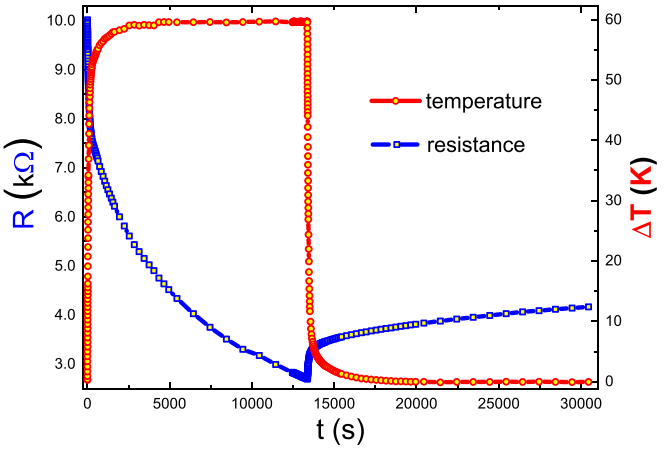

FIG. 1. A typical protocol used in thermal treating In_xO films. Resistance data $R(t)$ are shown in squares and refer to the left scale, the sample temperature above room's $\Delta T(t) \equiv T(\text{heater})\text{-}T(\text{room temperature})$ is plotted with circles and refer to the right scale. The sample here has $N \approx 8.5\times10^{20}$ cm^{-3}, thickness of 52 nm and lateral dimension of 1×1 mm^2.

grazing-angle x-ray technique [22]. It was further correlated with *in situ* resistivity and optical-spectroscopy measurements [22]. For In_xO, a system with the Fermi energy in the conduction band, higher density typically yields higher mobility. This may be due to the enhanced overlap of wave functions and improved connectivity. It will be shown below that there is more to the improved mobility than just densification.

The time-dependent processes that occur whereas the temperature is constant were qualitatively accounted for by a heuristic model based on the two-level-systems that make up the potential landscape of the disordered system [23]. A similar approach was used in Ref. [24] to offer a platform for accounting for thermal expansion of glasses.

III. RESULTS AND DISCUSSION

A. Raman spectra

Figure 2 shows the measured Raman spectra of three batches of In_xO films before and after thermal treatment. The samples differ by their O-In ratio determined during the deposition process. They are identified in the figure by their carrier-concentration N measured by the Hall effect. These three compositions were chosen to represent the high-N, medium-N, and low-N versions of In_xO. The high-N and low-N versions of In_xO, in particular, exhibit different behavior in transport [20], and as will be shown below, they differ in terms of other material properties. To cater for the spatial intensity variations of the scattered signal the Raman spectra were normalized to the intensity of the as-made sample evaluated at 450 cm^{-1} (averaged value over the interval 440–450 cm^{-1}). This will be referred to as a "background" intensity I_0. The ratio I_P/I_0, where I_P is the intensity at the BP maximum, turns out to be a meaningful measure of the BP magnitude; I_0 taken at different points across a given specimen may vary by more than $\approx$30% whereas I_P/I_0 appears to be constant to better than 2%.

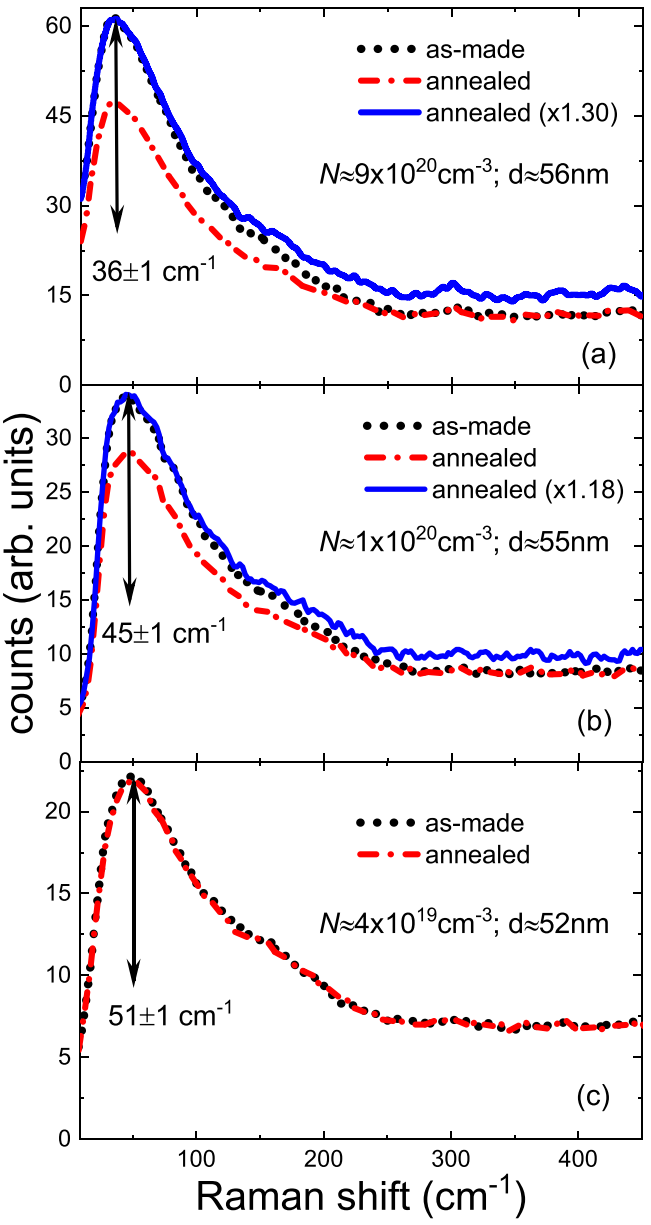

FIG. 2. The Raman spectra for the three studied batches of In_xO measured down to $\approx$10 cm^{-1} with a laser wavelength $\lambda = 532$ nm. Spectra are shown before and after heat treatment. The Ioffe-Regel parameters $k_F\ell$ for these samples are as folows: (a) before 0.11; after 0.39, (b) before 0.12; after 0.41, (c) before 0.078; after 0.42. Blue curves are scaled-up copies of the heat-treated spectra (the factor is chosen to match the intensity reading at the peak). Note that the heat-treated curve shows a wider high-energy tail than the as-made samples of both sample (a) and sample (b).

Qualitatively, the Raman spectra for the three batches in Fig. 2 exhibit the same BP shape characteristic of other amorphous and glassy systems [3–16]. There are, however, two quantitative differences depending on the composition of the material. First, the peak position increases with the O-In ratio (Fig. 3). The position of the BP scales with the typical phonon energy of the material which is naturally smaller for the In-richer In_xO, so this is just a consequence of the batch composition. That the peak position appears at a frequency

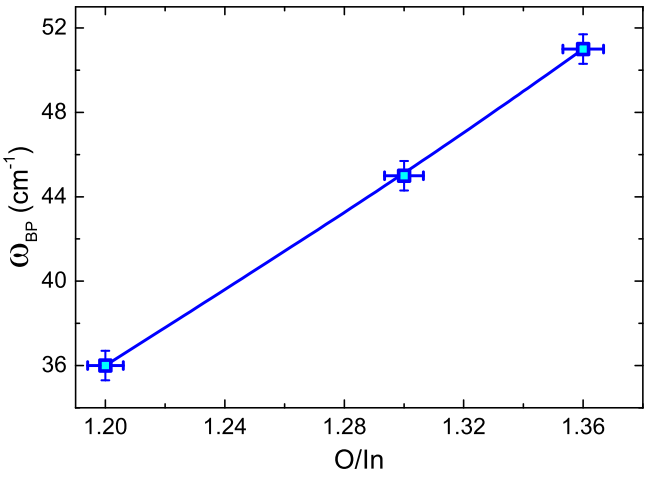

FIG. 3. The dependence of the energy of the BP maximum ω_{BP} on the In_xO composition O/In. This is obtained through the relation between N and the oxygen/indium mass ratio studied elsewhere (Fig. 6 in Ref. [19]).

ω_p(O/In) and does not shift due to the thermal treatment is consistent with the finding that the Hall coefficient is unchanged in the process [2].

Second, the heat treatment causes a more conspicuous decrease in the BP magnitude for the higher-N version whereas having an indistinguishable change in the spectra of the low-N version despite the comparable change in the samples resistance during annealing. Also, for a comparable conductivity, the relative magnitude of the BP, is larger the higher is the carrier concentration.

The amount of disorder required to affect a given change in the conductivity (or $k_F\ell$) in a degenerate Fermi system, such as In_xO grows with the Fermi energy (thus, with N). This correlation was demonstrated in the dependence of the optical gap on $k_F\ell$ studied *in situ* in Ref. [2]. Figure 4 shows three curves from this paper for samples with carrier concentration that are close to these of the batches studied in Fig. 2. Note that for a comparable change in $k_F\ell$ a larger change in the optical gap occurred for the sample with the higher carrier concentration, a similar trend to that observed in the dependence of the BP on disorder (Fig. 2). The relative change in the BP magnitude presumably reflects the degree of the structural change that occurred during heat treatment. The correlation between disorder (either chemical or electronic) and I_P/I_0 (Table I) has the same reason—for a comparable $k_F\ell$

TABLE I. Values of parameters for the three In_xO batches measured in Fig. 2. The electronic disorder (characterized by $k_F\ell$) includes the contribution of the deviation from stoichiometry that is relevant for phonon scattering vs electron scattering discussed in the text below. Note the systematic dependence of the BP magnitude on the batch disorder.

δ [O/In]	W_C (eV)	I_P/I_0 as made	I_P/I_0 annealed
0.3	2.21	5.3	4.2
0.2	0.51	4.1	3.4
0.14	0.28	3.1	3.1

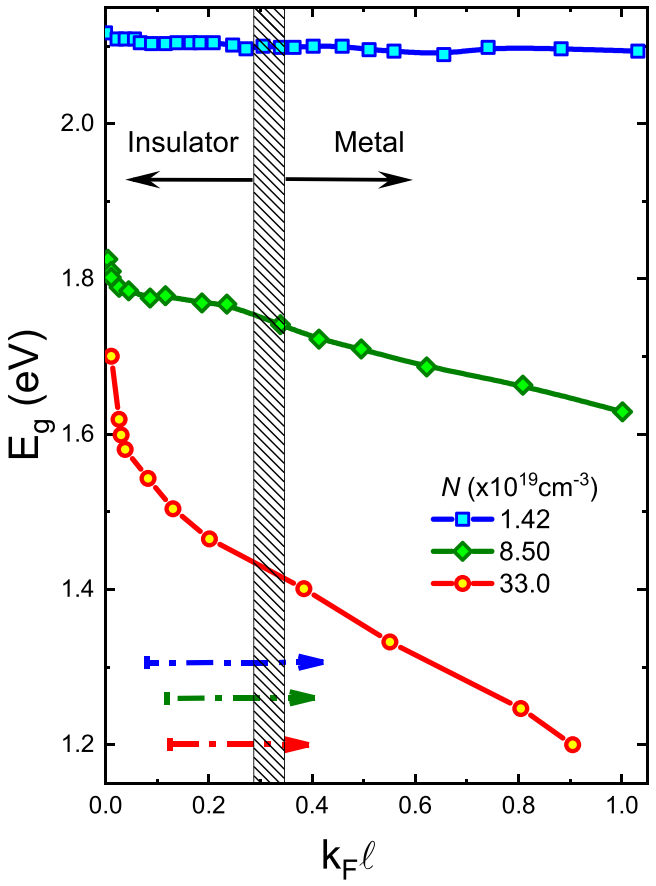

FIG. 4. The dependence of the optical gap on the Ioffe-Regel parameter $k_F\ell$ for different versions of In_xO labeled by their carrier concentration. Note that a larger change in E_g is required to affect a given change in $k_F\ell$ the larger N is. The arrows mark the value of $k_F\ell$ for the as-made and annealed states of the three samples of Figs. 2; red, 2(a), green, 2(b), and blue, 2(c).

higher disorder yields a more conspicuous BP demonstrating the common observation related to the phenomenon [12].

Table I includes the relative magnitude of the BP before and after annealing with the batch chemical-disorder δ[O/In] and a quantitative measure of disorder W_C based on data of electronic transport. The chemical disorder is taken here as the deviation of the composition from that of the stoichiometric In_2O_3 compound. W_C is the critical disorder that Anderson localizes the particular batch. $W_C \propto E_F \propto N^{2/3}$ where E_F is the Fermi energy. For In_xO the proportionality factor between disorder and Fermi energy was found to be as follows: $W_C \simeq 6.2E_F$ [2] and E_F of a given batch is obtained using free-electron formulas.

B. Structural changes resulting from the heat treatment

Before proceeding with further analysis of the Raman spectra we digress now to see what actually changes in the system microstructure due to heat treatment. This was performed by using customary tools of structural analysis; x-ray and electron microscopies. Special emphasis was given to the high-N version of In_xO where the effect in terms of Raman spectroscopy is manifestly large. Consider first the

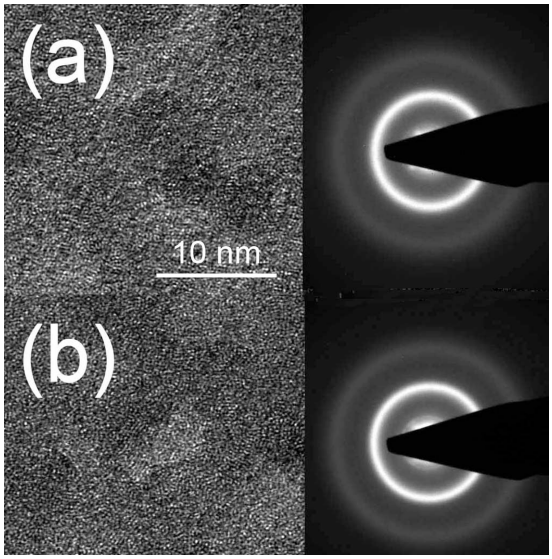

FIG. 5. Bright-field TEM images and the associated diffraction patterns for a 20-nm-thick In_xO sample deposited on a carbon-coated Cu grid. (a) An as-made sample and (b) the same sample after heat treatment. The control sample, deposited on a glass substrate, had a $k_F\ell$ of 0.16 and 0.39 before and after treatment, respectively.

electron-diffraction and TEM images for a typical sample shown in Figs. 5(a) and 5(b): Both diffraction patterns exhibit broad rings characteristic of amorphous structure with no sign of crystallization. In fact, it is hard to see a difference in the before and after patterns. On closer examination, the first strong ring in the pattern is sharper in the annealed sample, and the associated bright-field image appears somewhat softer.

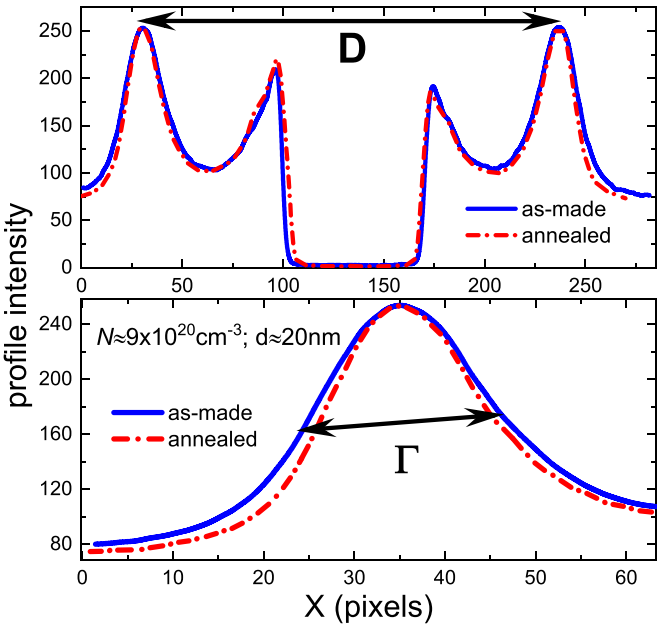

FIG. 6. Intensity profile for the two diffraction patterns shown in Fig. 5. Top: Scanned across the first strong ring diameter D. Bottom: The profile of the first strong ring clearly showing the change in the width Γ after heat treatment.

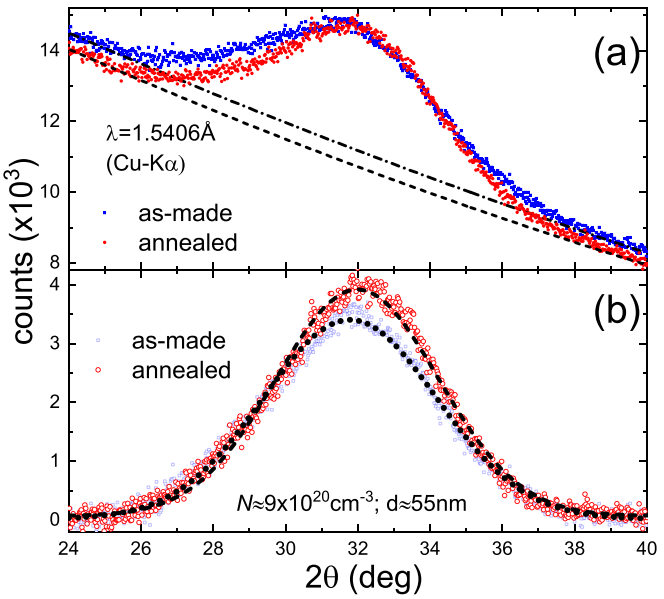

FIG. 7. X-ray diffraction taken over the first strong diffraction ring of the sample that had $k_F\ell = 0.09$ and $k_F\ell = 0.38$ for as-made and annealed samples, respectively. (a) Are the raw data, and the dashed and dotted lines stand for the background intensities. These background lines are subtracted from the raw data and fitted in (b) to $A\exp[-0.5(\frac{X-X_0}{\sigma})^2]$ where A is the intensity amplitude and $X \equiv 2\theta$. The fits, shown as dashed lines, yield $X_0 = 31.78 \pm 0.008$; $\sigma = 2.4 \pm 0.01$ and $X_0 = 31.98 \pm 0.008$; $\sigma = 2.2 \pm 0.01$ for the as-made and annealed plots, respectively. The larger intensity at the peak (bottom graph) is due to the reduced background and the narrower line width.

The changes in the diffraction pattern may be quantified by recording the intensity profiles of the diffraction patterns as illustrated in Fig. 6. The measurement confirms the eye impression; the width of the ring Γ decreased by ≈12% in the annealed sample. At the same time, the average ring diameter indicated by D in the figure, *increased* by $\approx 0.4 \pm 0.1\%$ suggesting a reduced interatomic separation due to annealing.

Similar results were obtained from XRD measurements on this high-N sample as shown in Fig. 7. The small differences between the XRD and the electron diffraction in terms of the changes in D and ring width may be due to the different substrates used.

On the basis of these measurements one might conclude that the volume-change $-\Delta V/V$ of this sample due to the thermal treatment is on the order of 1.2%–1.8%. However, the results of the XRR measurement suggest that $\Delta V/V$ for this sample may be significantly larger [Fig. 8(a)]; Following treatment the sample thickness was reduced by ≈3.3% implying a volume-change $-\Delta V/V$ of the order of ≈10%. Similar $-\Delta V/V$ values during heat treatment were obtained in a previous study of In_xO [2]. The difference in $-\Delta V/V$ derived from the XRD versus that of the XRR suggest that the In_xO structure is made up of loosely packed aggregates of relatively dense material. Such a porous medium is common in vapor-deposited films and more generally in substances that were quench cooled from high temperatures. Actually, porosity is an abundant property of many materials. An extreme example

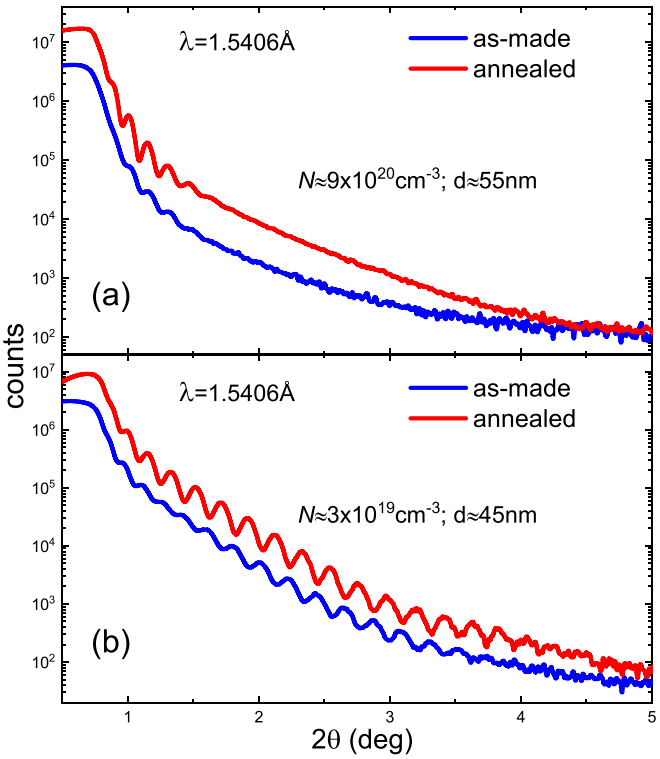

FIG. 8. X-ray reflectometry for two versions of In_xO films having similar composition as that of the samples in Fig. 2. Plots are shown for the before-and-after heat treatment (curves are displaced along the ordinate for clarity). The thickness of the sample in (a) changed during heat treatment from 56.2 ± 0.1 to 54.5 ± 0.1 nm and the sample in (b) changed from 45.1 ± 0.1 to 45 ± 0.1 nm. The films roughness parameters are: 1 ± 0.2 for the sample in (a) and 0.4 ± 0.1 for the sample in (b).

of such a structure is a cotton ball or a bundle of steel wool. The volume of these substances may be greatly reduced when pressed whereas their solid part remains essentially intact.

Figure 8(b) shows the XRR trace taken of a low-N sample that was added for comparison. It exhibits a quantitatively different behavior than the high-N sample in two aspects; the visibility of the interference extends over a wider range of angles, and the change in thickness during heat treatment is much smaller (per the same change in the sample resistance). Note that heat treatment enhanced the interference visibility in both samples yet the low-N sample retains a smoother film surface even when its resistance is considerably higher. Evidently, for a similar $k_F\ell$, the high-N version of In_xO is both, more disordered and has a rougher surface.

To understand how structural aspects affect conductivity and the BP it may be useful to review the specific ingredients responsible for scattering in In_xO films.

C. The elements of disorder in amorphous indium-oxide films and their effect on conductivity and the boson peak

As amorphous material In_xO lacks long-range order which by itself imposes limit on charge mobility. The vacuum-deposited In_xO films have ancillary sources of disorder that lead to scattering and restrict their $k_F\ell$ value. First, there is an off-diagonal disorder in the material that is related to the distributed nature of the interatomic separation. The distribution of interparticle distances gets narrower as the volume decreases and the system approaches the "ideal" closed-packed amorphous structure. This enhances wave-function overlap and, therefore, it naturally affects the conductivity. The diminishment of off-diagonal disorder during heat treatment is clearly reflected in the reduced width of the electron diffraction and in the XRD patterns (Figs. 5–7, respectively). The latter has been often associated with the appearance of medium-range order in the system [7]. This restructure process is also reflected in the rate distribution of the glass dynamics [23]. The "free volume" of the sample that is presumably eliminated is probably the most important single element in giving rise to phonon scattering. In fact, a porous nature of amorphous structures has been shown by detailed simulation studies to be the major contributing factor in the BP magnitude [12].

A clear correlation between a structural change and a modified BP is manifested in our paper whenever a significant change in density takes place. This is observed most conspicuously for the heat-treated high-N sample where density is reduced by $\approx 10\%$ [Fig. 8(a)] and the Raman spectrum shows a $\approx 30\%$ reduction in magnitude [Fig. 2(a)]. The correlation with the material density follows the trend reported in experiments on other disordered systems where the magnitude of the BP was observed to be smaller following densification by pressure [25–34].

The main difference between heat treatment and applying high pressure appears to be the shift of the BP position to higher energy in the pressure experiments [25–34] whereas no such shift is encountered in the Raman spectra for the thermally annealed samples. In this regard the evolution of the BP shape in our experiments followed the heterogeneously distributed elastic constants scenario described by Schirmacher and Ruocco [8]. A similar behavior to our annealing experiments was observed in the BP spectra of As_2S_3 samples after it was cold quenched from a well-annealed state [35].

Another source of disorder in the amorphous indium-oxide system is associated with deviation from stoichiometry—chemical disorder. Relative to the ionic compound In_2O_{3-x}, there are 5–30% oxygen vacancies in In_xO spanning the range of $\approx 10^{18}$–5×10^{21} cm^{-3} in terms of carrier concentration. To preserve chemical neutrality some indium atoms must assume a valence of $+1$ instead of the $+3$ they have in the stoichiometric compound. When randomly distributed this valence fluctuation forms a background potential with an amplitude on the order of few eV (assuming an average interatomic separation on the order of ≈ 0.3 nm). This type of disorder is quite prevalent in nonstoichiometric compounds, metallic-oxides, high-Tc materials, etc., and it seems to be a main source of elastic scattering in both In_xO and In_2O_{3-x} [36]. On the other hand, the role chemical disorder plays in the buildup of a BP is unclear. Deviation from stoichiometry unaccompanied by other factors, does not necessarily promote formation of a BP; polycrystalline films of In_2O_{3-x} exhibits 5–8% oxygen vacancies [36] whereas showing very small magnitude of BP relative to the amorphous version [21]. This probably means that oxygen vacancies and larger pockets of free volume, such as divacancies, are evenly distributed such

that density fluctuations over a phonon wavelength are rather small.

Finally, the reduction of surface roughness during the heat treatment revealed in the XRR data needs elaboration. Changes in the interference visibility presumably reflect rearrangement of ions at the film surface. This seems to occur even when changes in thickness were too small to be observed [see Fig. 8(b)]. In principle, a rough film surface is a source of scattering for both phonons and electrons, and it is natural to expect less scattering when the surface roughness is reduced. Given that the mean-free-path ℓ in our samples is much smaller than the film thickness, the contribution of the surface to scattering by either electrons or phonons is probably very small. Electrical conductivity is sensitive enough to detect a small change in disorder in the sample. For phonons, however, the same structural change may be too small to affect the BP magnitude [Fig. 2(c)]. In other words, a measurable change in conductivity may be affected without a significant structural change in a similar vein with the dependence of the optical-gap E_g on $k_F\ell$ for a low-N sample where E_g remains almost constant whereas $k_F\ell$ changes over a large range (Fig. 4).

IV. SUMMARY

We have followed by transport, structural tools, and Raman spectroscopy the changes that occur during heat-treating In_xO films. Transport measurements were used to quantify the degree of disorder in In_xO samples with different carrier concentrations before and after treatment. The disorder is characterized by assigning each sample a Ioffe-Regel parameter $k_F\ell$. The study reveals a correlation between the system disorder defined in this way and the magnitude of the BP. This correlation suggests that, in these systems, phonons are scattered by the same elements of disorder that cause scattering of electrons although not necessarily with the same efficiency.

An element of disorder that has a large effect on the BP magnitude is the presence of "free volume" in the system that in In_xO is presumably related to the spatial distribution of oxygen vacancies. These are rearranged during the annealing process to reduce the system volume, and the BP magnitude is changed accordingly. Our study furnishes the experimental support to the simulation work of Shintani and Tanaka that identified the most conspicuous BP in low-density defective structures [12]. This led them to conclude: "*...the origin of the boson peak (are) transverse vibrational modes associated with low-density defective structures*" [12].

The emerging picture is that heat-treating In_xO is analogous to the process of gently tapping a ground-coffee bag to pack it tighter. Tapping supplies the energy necessary to overcome local barriers allowing the powder to reduce its gravitational energy. Temperature and the interparticle attraction, respectively, play the analogous roles in the process of densifying In_xO. Enhanced conductivity due to densification follows from enhanced wave-function overlap as well as from improved connectivity. This is accompanied by a reduced disorder and, therefore, weaker heterogeneity which is reflected in a smaller magnitude of the BP. The flexibility that the In_xO system offers in terms of fine-tuning disorder by heat treatment makes it a prime candidate for the study of electronic transport in glasses and as demonstrated in this paper, also for other fundamental properties of amorphous materials.

ACKNOWLEDGMENTS

We benefited from discussions with W. Schirmacher and A. Zaccone. The assistance of A. Radko, V. Uvarov, and I. Popov from the Center for Nanoscience and Technology (HU) is gratefully acknowledged. This research has been supported by the 1030/16 Grant administered by the Israel Academy for Sciences and Humanities.

[1] H. Wiesmann, M. Gurvitch, A. K. Ghosh, H. Lutz, O. F. Kammerer, and M. Strongin, Estimate of density-of-states changes with disorder in A-15 superconductors, Phys. Rev. B **17**, 122 (1978); M. Gurvitch, A. K. Ghosh, H. Lutz, and M. Strongin, Low-temperature resistivity of ordered and disordered A15 compounds, *ibid.* **22**, 128 (1980); M. Putti, R. Vaglio, and J. Rowell, Radiation damaged MgB_2: A comparison with A15 superconductors, J. Phys.: Conf. Ser. **97**, 012327 (2008).

[2] Z. Ovadyahu, Memory versus irreversibility in the thermal densification of amorphous glasses, Phys. Rev. B **95**, 214207 (2017).

[3] V. K. Malinovsky, V. N. Novikov, P. P. Parshin, A. P. Sokolov, and M. G. Zemlyanov, Universal form of the low-energy (2 to 10 meV) vibrational spectrum of glasses, Europhys. Lett. **11**, 43 (1990).

[4] S. R. Elliott, A unified model for the low-energy vibrational behavior of amorphous solids, Europhys. Lett. **19**, 201 (1992).

[5] W. Schirmacher, G. Diezemann, and C. Ganter, Harmonic Vibrational Excitations in Disordered Solids and the "Boson Peak", Phys. Rev. Lett. **81**, 136 (1998).

[6] N. N. Ovsyuk and V. N. Novikov, Influence of structural disorder on Raman scattering in amorphous porous silicon, Phys. Rev. B **57**, 14615 (1998).

[7] S. Sugai and A. Onodera, Medium-Range Order in Permanently Densified SiO_2 and GeO_2 Glass, Phys. Rev. Lett. **77**, 4210 (1996).

[8] W. Schirmacher and G. Ruocco, Heterogeneous elasticity: The tale of the boson peak, arXiv:2009.05970 [Contributed chapter to *Low-Temperature Thermal and Vibrational Properties of Disoredered Solids* (A Half-Century of universal "anomalies" of glasses), edited by M. A. Ramos (to be published)].

[9] S. N. Taraskin and S. R. Elliott, Phonons in vitreous silica: Dispersion and localization, Europhys. Lett. **39**, 37 (1997).

[10] J. S. Lannin, N. Maley, and S. T. Kshirsagar, Raman scattering and short range order in amorphous germanium, Solid State Commun. **53**, 939 (1985).

[11] M. Baggioli and A. Zaccone, Unified theory of vibrational spectra in hard amorphous materials, Phys. Rev. Res. **2**, 013267 (2020).

[12] H. Shintani and H. Tanaka, Universal link between the boson peak and transverse phonons in glass, Nat. Mater. **7**, 870 (2008).

[13] V. Lubchenko and P. G. Wolynes, The origin of the boson peak and thermal conductivity plateau in low-temperature glasses, Proc. Natl. Acad. Sci. USA **100**, 1515 (2003).

[14] S. N. Taraskin, Y. L. Loh, G. Natarajan, and S. R. Elliott, Origin of the Boson Peak in Systems with Lattice Disorder, Phys. Rev. Lett. **86**, 1255 (2001).

[15] K. Niss, B. Begen, B. Frick, J. Ollivier, A. Beraud, A. Sokolov, V. N. Novikov, and C. Alba-Simionesco, Influence of Pressure on the Boson Peak: Stronger than Elastic Medium Transformation, Phys. Rev. Lett. **99**, 055502 (2007).

[16] H. R. Schober, U. Buchenau, and V. L. Gurevich, Pressure dependence of the boson peak in glasses: Correlated and uncorrelated perturbations, Phys. Rev. B **89**, 014204 (2014).

[17] N. F. Mott and A. E. Davis, *Electronic Processes in Non-Crystalline Materials* (Oxford University Press, London, 1971).

[18] K. A. Blanks, The role of the Raman coupling coefficient in an inelastic light scattering process in amorphous solids, J. Non-Cryst. Solids **208**, 81 (1996); A. Fontana, R. Dell'Anna, M. Montagna, F. Rossi, G. Viliani, G. Ruocco, M. Sampoli, U. Buchenau, and A. Wischnewski, The Raman coupling function in amorphous silica and the nature of the long-wavelength excitations in disordered systems, Europhys. Lett. **47**, 56 (1999); B. Schmid and W. Schirmacher, Raman Scattering and the Low-Frequency Vibrational Spectrum of Glasses, Phys. Rev. Lett. **100**, 137402 (2008).

[19] D. Shahar and Z. Ovadyahu, Superconductivity near the mobility edge, Phys. Rev. B **46**, 10917 (1992).

[20] U. Givan and Z. Ovadyahu, Compositional disorder and transport peculiarities in the amorphous indium-oxides, Phys. Rev. B **86**, 165101 (2012).

[21] See Supplemental Material at http://link.aps.org/supplemental/10.1103/PhysRevMaterials.5.085602 for fuller details of the two setups used for Raman spectroscopy and associated data.

[22] Z. Ovadyahu, Slow dynamics of the electron-glasses; the role of disorder, Phys. Rev. B. **95**, 134203 (2017).

[23] Z. Ovadyahu, Structure dynamics in thermal-treatment of amorphous indium-oxide films, Phys. Status Solidi B **257**, 1900310 (2020).

[24] Y. M. Galperin, V. L. Gurevich, and D. A. Parshin, Theory of low-temperature thermal expansion of glasses, Phys. Rev. B **32**, 6873 (1985).

[25] L. Orsingher, A. Fontana, E. Gilioli, G. Carini, G. Carini, G. Tripodo, T. Unruh, and U. Buchenau, Vibrational dynamics of permanently densified GeO_2 glasses: Densification-induced changes in the boson peak, J. Chem. Phys. **132**, 124508 (2010).

[26] T. Deschamps, C. Martinet, D. de Ligny, J. L. Bruneel, and B. Champagnon, Correlation between boson peak and anomalous elastic behavior in GeO_2 glass: An *in situ* Raman scattering study under high pressure, J. Chem. Phys. **134**, 234503 (2011).

[27] J. Schroeder, W. Wu, J. L. Apkarian, M. Lee, L.-G. Hwa, and C. T. Moynihan, Raman scattering and Boson peaks in glasses: Temperature and pressure effects, J. Non. Cryst. Solids **349**, 88 (2004).

[28] M. Ahart, D. Aihaiti, R. J. Hemley, and S. Kojima, Pressure dependence of the Boson peak of glassy glycerol, J. Phys. Chem. B **121**, 6667 (2017).

[29] B. Mantisi, S. Adichtchev, S. Sirotkin, L. Rafaelly, L. Wondraczek, H. Behrens, C. Marcenat, N. V. Surovtsev, A. Pillonnet, E. Duval, B. Champagnon, and A. Mermet, Non-Debye normalization of the glass vibrational density of states in mildly densified silicate glasses, J. Phys.: Condens. Matter **22**, 025402 (2010).

[30] V. L. Gurevich, D. A. Parshin, and H. R. Schober, Pressure dependence of the boson peak in glasses, Phys. Rev. B **71**, 014209 (2005).

[31] L. Hong, B. Begen, A. Kisliuk, C. Alba-Simionesco, V. N. Novikov, and A. P. Sokolov, Pressure and density dependence of the boson peak in polymers, Phys. Rev. B **78**, 134201 (2008).

[32] M. Zanatta, G. Baldi, S. Caponi, A. Fontana, E. Gilioli, M. Krish, C. Masciovecchio, G. Monaco, L. Orsingher, F. Rossi, G. Ruocco, and R. Verbeni, Elastic properties of permanently densified silica: A Raman, Brillouin light, and X-ray scattering study, Phys. Rev. B **81**, 212201 (2010).

[33] A. Monaco, A. I. Chumakov, G. Monaco, W. A. Crichton, A. Meyer, L. Comez, D. Fioretto, J. Korecki, and R. Rüffer, Effect of Densification on the Density of Vibrational States of Glasses, Phys. Rev. Lett. **97**, 135501 (2006).

[34] E. Stavrou, C. Raptis, and K. Syassen, Effects of pressure on the boson peak of tellurite $(TeO_2)_{1-x}(ZnO)_x$ glasses: Evidence of an elastic glass-to-glass transition, Phys. Rev. B **81**, 174202 (2010).

[35] V. K. Malinovsky and A. P. Sokolov, The nature of the boson peak in Raman scattering in glasses, Solid State Commun. **57**, 757 (1986).

[36] Z. Ovadyahu, B. Ovryn, and H. W. Kraner, Microstructure and electro-optical properties of evaporated indium-oxide films, J. Elect. Chem. Soc. **130**, 917 (1983).